A Neural Network Based Analytical Model for Predicting Acoustic Noise in Synchronous Reluctance Motors

Bofan Wang

Department of Electrical & Computer Engineering
McGill University
Montreal, Canada

Janurary 2017

A thesis submitted to McGill University in partial fulfillment of the requirements for the degree of Master Degree.

2017/04/16

Abstract

Synchronous Reluctance Motors (SynRMs) have become more and more popular as a substitute for PMSMs for traction applications due to the lack of rare earth permanent magnets in their structure. Considering the noise and vibration, reluctance motors are known to have relatively inferior performance, i.e. they can be quite loud. In this case, developing design guidelines for mitigating noise and vibration levels is very important for these machines. Developing comprehensive guidelines, i.e. design knowledge, on the effects of modifying any geometrical, electrical or winding related variable on SynRM loudness is a significant challenge. Based on studies of other machines, a systematic study on the effects of changing some important design variables on SynRMs can be applied.

This thesis proposes a neural network based prediction model for estimating the loudness level in a SynRM using an electromagnetic simulation model. We calculated the natural mode frequencies of several stator models corresponding to different geometric configurations. Then, we used a Generalized Regression Neural Network (GRNN) to predict the natural mode frequencies of the stators. The slot number, tooth width, slot depth, tooth tip thickness and tang angle were the inputs to this neural network. We obtained the airgap flux density values using the Infolytica software MagNet. Then, we successfully calculated the predicted loudness level value of the SynRM models by using an analytical method. Finally, we discussed some parameters which influence the loudness.

Résumé

Les moteurs synchrones de réluctance (SynRM) sont devenus de plus en plus populaires en tant que substitut aux PMSM pour les applications de traction en raison de l'absence d'aimants permanents de terres rares dans leur structure. En considérant le bruit et la vibration, on sait que les moteurs à réluctance ont une performance relativement inférieure, c'est-à-dire qu'ils peuvent être très forts. Dans ce cas, l'élaboration de directives de conception pour atténuer le bruit et les vibrations est très importante pour ces machines. L 'élaboration de directives complètes, c'est - à - dire les connaissances de conception, sur les effets de la modification de toute variable géométrique, électrique ou liée à l' enroulement sur la sonorité SynRM est un défi important. Sur la base d'études d'autres machines, une étude systématique des effets de la modification de certaines variables de conception importantes sur les SynRM peut être appliquée.

Cette thèse propose un modèle de prédiction basé sur le réseau neuronal pour estimer le niveau de loudness dans une SynRM en utilisant un modèle de simulation électromagnétique. Nous avons calculé les fréquences en mode naturel de plusieurs modèles de stators correspondant à différentes configurations géométriques. Ensuite, nous avons utilisé un réseau neuronal de régression généralisée (GRNN) pour prédire les fréquences en mode naturel des stators. Le nombre de fentes, la largeur des dents, la profondeur de la fente, l'épaisseur de la pointe de la dent et l'angle de tangage étaient les entrées de ce réseau de neurones. Nous avons obtenu les valeurs de densité de flux d'airgap en utilisant le logiciel Infolytica MagNet. Ensuite, nous avons calculé avec succès la valeur de niveau d'intensité prédite des modèles SynRM en utilisant une méthode analytique. Enfin, nous avons discuté de certains paramètres qui influent sur le volume sonore.

Statement of Previous Paper

This thesis includes the work of the paper: Bofan Wang, Tanvir Rahman, Kang Chang, Mohammad Hossain Mohammadi, David A. Lowther. ”A neural network based surrogate model for predicting noise in synchronous reluctance motors”, 2016 IEEE Conference on Electromagnetic Field Computation (CEFC).

In this paper, Bofan Wang is the main author who implements the main experiments and theoretical derivation. Dr. Tanvir Rahman and Dr. David A. Lowther kindly gave their suggestions and constructive comments during this work. Mr. Kang Chang provided natural mode frequencies data and Mr. Mohammad Hossain Mohammadi provided the data of flux density.

Acknowledgments

I would like to dedicate my deepest gratitude to my research advisor, Prof. David A Lowther, for his long-term supervision of my academic life and constructive suggestion and criticism for my thesis. Also, this thesis won't be successfully finished without Dr. Tanvir Rahman's direction. I really appreciate for his help.

To my colleagues, Dr. Min Li, Mr. Rodrigo César Pedrosa Silva, Mr. Mohammad Hossain Mohammadi, Ms. Linwan Liu and Mr. Kang Chang. I will always remember your kind support and inspiration for me and the happy time we get together.

A special appreciation to my friend, Mr. Jian. Hui, I will always remember your devoted help and encouragements. *"For he today who sheds his blood with me shall be my brother."*

Moreover, I want to say thank you to my beloved family. To my aged grand parents and my parents. Without your love and support, I won't make any achievements in my life so far. Chinese people are always too shy to express their love to their family, I should thank the acknowledgments part in the thesis give me this chance to say"I love you all so much."

Contents

List of Figures

List of Tables

List of Acronyms

Acronyms	Description
AC	Alternating Current
BP	Back Propagation
BPNN	Back Propagation Neural Network
DC	Direct Current
ANN	Artificial Neural Network
FEA	Finite Element Analysis
FOC	Field-Oriented Control
GRNN	Generalized Regression Neural Network
HEV	Hybrid Electric Vehicle
IPM	Interior Permanent Magnet
NN	Neural Network
PDF	Probability Density Function
PM	Permanent Magnet
PMSM	Perment Magnet Synchronous Reluctance Motor/Machine
RBF	Radial Basis Function
RBNN	Radial Basis Neural Network
RMSRE	Root Mean Square Relative Error
SMPM	Surface-Mounted Permanent Permanent Magnet

SPL	Sound Pressure Level
SWL	Sound Power Level
SRM	Switched Reluctance Motor/Machine
SynRM	Synchronous Reluctance Motor/Machine
TLA	Transversally-Laminated Anisotropic

List of Symbols

Symbols	**Description**
A_i	radial displacement of the i_{th} mode
A_{i_n}	radial displacement excited by n_{th} order force under i_{th} mode
B	flux density
B_r	radial component of the flux density
B_t	tangential component of the flux density
c	speed of sound
D_i	inner diameter of the stator
f_e	harmonic excitation frequency
f_m	natural mode frequency
F	force
F_r	radial force
L_f	stack length of the stator
L_w	loudness level
M	mass of the stator
N_p	number of poles
P	pressure
P_r	radial pressure
R_i	inner radius of the stator

S_i	area of the inner surface of the stator
W_b	width of rotor flux barrier
W_c	width of rotor flux carrier
α	rotation angle
μ_0	magnetic permeability
ω_r	rotor rotational speed
ζ_m	damping factor
ρ	air density

Chapter 1

Introduction

1.1 Motivation

It is estimated that more than 65% of the electrical energy produced in developed countries is consumed by electric motors which are often embedded in larger systems as an integral part. Their noise immensely affects the overall noise of the system, [1] and its mitigation is also a significant design challenge for the machines. The sources of the noise are the electromagnetic force, which is the dominating one, the mechanical force and aerodynamic. [2] In order to calculate the loudness, a series of electromagnetic and structural simulations are required which are computationally time-consuming. In this case, building a computationally efficient prediction model which can estimate the loudness level of the noise of the motor is necessary, as it can not only help identify the optimal parameters for less noisy motors but also be good for reducing the noise and vibration levels, which can bring environmental benefits.

Synchronous Reluctance Motors (SynRMs) have become more and more popular as a substitute for Permanent Magnet Synchronous Motors (PMSMs) for traction applications due to the lack of rare earth permanent magnets in their structure. However, they can be quite loud. A noiseless environment is an important factor in a healthy lifestyle. This research may help in this area by predicting the noise level caused by electromagnetic sources in SynRMs.

1.2 Introduction to Loudness

In physics, sound is a vibration that propagates an audible mechanical wave of pressure and displacement, through a medium such as air or water. In physiology, sound is the sensation of such waves by the brain.

Loudness is the characteristic of a sound. And it is also primarily a correlate of physical strength (amplitude). “More formally, it is defined as that attribute of auditory sensation in terms of which sounds can be ordered on a scale extending from quiet to loud” [3]. The Decibel (dB) is the unit of the loudness and can be calculated by *Sound Pressure Level* (SPL) or *Sound Power Level* (SWL).

The defination of the decibel is [4]:

$$dB = 10log_{10}(\frac{SPL}{\text{Reference Level}}) \tag{1.1}$$

or

$$dB = 10log_{10}(\frac{SWL}{\text{Reference Level}}) \tag{1.2}$$

Here, the unit of SPL is the Pascal, and the unit of SWL is the Watt. According to [2], [5] and [4] : For SPL, the reference level is $2 \times 10^{-5} Pascals$, for SWL, the reference level is $10^{-12} Watts$. The reference level is a constant which can help us to compute the loudness level. As we know from the above that loudness is a correlate of physical strength (amplitude), so it makes sense that the units of pressure (Pascal) or power (Watt) are brought in to calculate the value of loudness.

1.3 Research Background

In the study done by Rakib Islam and Iqbal Husain in 2010 [2], they discussed the noise and vibration in PMSM motors caused by electromagnetic forces and how to calculate the loudness. They used 9slot/6pole (9s6p), 12slot/10pole (12s10p), 12slot/8pole (12s8p) and 27slot/6pole (27s6p) motors as examples, proposing a procedure to calculate the magnetic forces on the stator teeth. Then they developed an analytical model that predicted the radial displacement of the stator teeth, and which can be used for calculating the sound power level. From their study, the formula to calculate the tangential and radial components of the forces was introduced. Using it, the instantaneous value of radial pressure can be obtained. Then their paper discusses the mode shapes and radial forces. Once the radial stress has been calculated, the radial displacement can be obtained. Meanwhile, they talk about how to calculate the sound power level of the acoustic noise by using the displacement. Finally, they use the sound pressure level to calculate the values of loudness. As a conclusion, the paper proposes an analytical model that uses radial displacement as the input to determine the sound power level then uses the sound power level to calculate the loudness value.

Following on from Rakib Islam and Iqbal Hussain's work, Mohammad S.Islam, Rakib Islam and Tomy Sebastian introduced an improved version [5]. In their research, they focus on PMSM motors in configurations such as 12slots/10poles, 9slots/6poles, 12slots/8poles, 15slots/10poles and 27slots/6poles. In the paper, the authors indicate the relationship between the displacement amplitude and the vibration mode orders for various slot/pole configurations. The main difference in these two papers is the method used to calculate the loudness value. Where [2]uses the sound power level , [5] uses the sound pressure level to calculate the loudness value.

In Jacek F. Gieras, Chong Wong, Joseph C S. Lai and Nesimi Ertugrul's work [6], they propose a procedure for a Permanent Magnet Brushless Motor (similar to a PMSM motor). As in the previous study, they also assume the magnetic force is the main source of the noise. From their research, it can be seen that the formulas of magnetic pressure in the air gap between the stator and the rotor are same as the ones given in [2] [5]. The procedure is approximately the same as [2], [5] using the displacement in the stator as an input to the model to calculate the loudness. To some extent, their research is better than the previous work because the authors show the formulas which calculate the amplitude of the stator more explicitly.

1.4 Synchronous Topologies

An **electric motor** consists of two main parts: a stationary stator comprised of excitation windings and a rotor free to rotate about its shaft or axis of rotation. A rotating magnetic field is generated by exciting the multiphase stator windings in a continuous or stepwise approach. Through the principle of electromechanical energy conversion [7], the rotor is forced to rotate and align itself with the stator magnetic axis thereby producing torque.

The total motor torque produced at a specific rotational speed can be subdivided into two torque components: the permanent magnet (PM) torque and the reluctance torque. The PM torque is produced by the interaction of the stator field with a fixed-magnitude rotor PM field, while the reluctance torque is generated by naturally aligning the rotor's magnetic axis with the stator's in order to minimize the overall reluctance of its magnetic flux path. Electric motors can be divided into different classes by different combinations of these two torque components, which can be seen in Fig. 1.1: (a)*Surface-Mounted Permanent-Magnet* (SMPM) motors which only produce PM torque, (b) and (c) Variable Reluctance motors which only produce reluctance torque, and (d) *Interior Permanent Magnet* (IPM) motors produce both torque components.

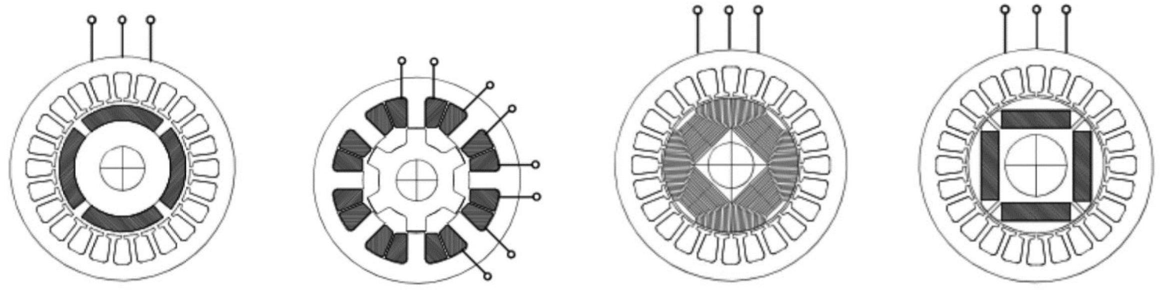

(a) Surface-Mounted PM AC Machine

(b) Switched Reluctance AC Machine

(c) Synchronous Reluctance AC Machine

(d) Interior PM AC Machine

Fig. 1.1 Cross-Sections of Selected Synchronous Electric Machines [8]

1.4.1 Permanent Magnet Machines

Most of the current Hybrid Electrical Vehicle (HEV) manufacturers utilize permanent magnet motors, such as SMPM or IPM motors. The PMs buried inside the rotor segment provide a constant rotor magnetic field which interacts with the stator field to produce PM torque at a given angular speed. The benefits of these machines are high torque-to-rotor volume density, efficiency levels and Constant Power Speed Range.

1.4.2 Variable Reluctance Machines

There are two main types of rotor structures shown under the Variable Reluctance Machine topology which is shown in Fig.1.2 [9]: (a) the *Switched Reluctance Motor* (SRM), (b) and (c) the *Synchronous Reluctance Motor* (SynRM). The only difference for (b) and (c) is their axis for stacking laminations. SRMs utilize a salient rotor with a salient stator, while the SynRMS use a salient rotor with a cylindrical stator. Salient stators consist of phase windings wound across individual stator poles, while cylindrical stators utilize sinusoidally-distributed windings similar to the Induction Machine (IM).

1.4.3 Synchronous Reluctance Motors

The Synchronous Reluctance Motor (SynRM) has a salient rotor structure and a cylindrical stator. It was first introduced by Kostko as the *reaction synchronous motor*, its stator produces a rotating field which is opposed to its doubly-salient SRM counterpart [10]. Kosto's rotor in Fig.1.3 [10] shows multiple iron laminations separated by insulated air layers to create a high magnetic saliency. Through an ideal set of sinusoidally-distributed coils excited by balanced sine wave currents, a smoothly-rotating stator field is produced in order to force the salient rotor to rotate and align its primary magnetic axis with the stator field. There have been various names of this singly-salient machine topology: *Synchronous Reluctance Machine* (SynRM), *Reluctance Synchronous Machine* (RSM) and *Reluctance Machine* (RM). In order to simplify, the name *Synchronous Reluctance Machine* is maintained throughout this thesis.

An asynchronous operation is required to raise the motor speed from zero before locking it to synchronism because this synchronous machine does not start at synchronous speed. One approach is to incorporate a squirrel-cage within the SynRM rotor to enable line-start operation through the electromagnetic induction principle. Different SynRM rotors with squirrel-cage structures are illustrated in Fig.1.4 [11] [12] (a),(b) and (c).

Due to the development of modern power electronics in the past decades, new motor

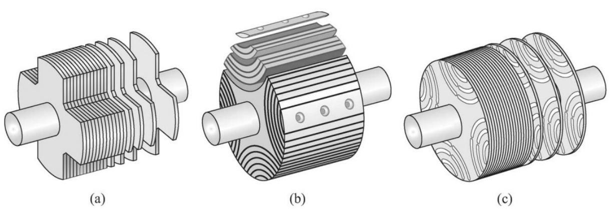

Fig. 1.2 Variable Reluctance Rotor Laminations :(a) Switched Reluctance Motor, (b) ALA Synchronous Reluctance Motor, (c) TLA Synchronous Reluctance Motor

[9]

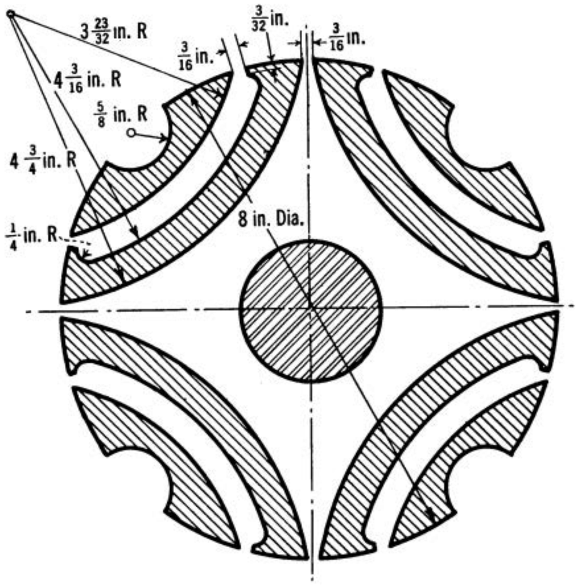

Fig. 1.3 Kostko's Rotor for the Reaction Synchronous Motor [10]

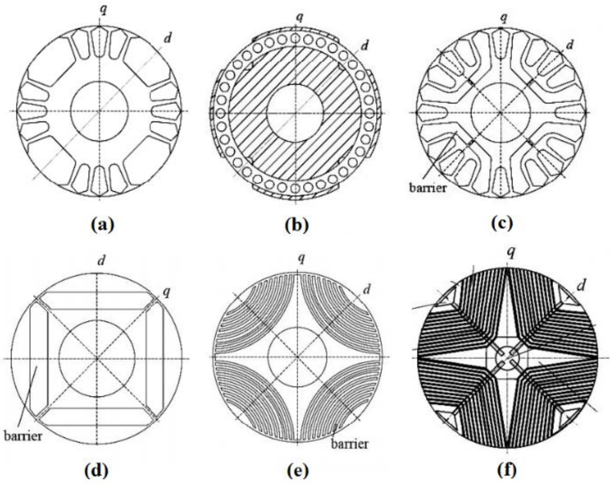

Fig. 1.4 Evolution of SynRM Rotor [11] [12]

control methods have been developed. For example, *Field-Oriented Control* (FOC), enabled variable frequency and motor speed operation. This FOC strategy eliminates the need for a line-start cage in exchange for a rotor position sensor or sensorless position techniques [13].

In Fig.1.4 [11] [12] (d),(e) and (f) utilize a high number of iron lamination and air insulation layers in an alternating manner to increase the rotor saliency and ability for sensorless position control.

1.5 Thesis Objectives

According to [2] [5] [6] the acoustic noise is generated from the radial displacement of the stator due to the electromagnetic force. The harmonics of the radial force can excite different stator modes, and each mode has its own shape. The mode shape of the stator is directly influenced by the natural mode frequency, [2] [5] [6]. Hence the amplitude of the radial displacement is a function of the natural mode frequency of the stator and the electromagnetic force in the air gap. Although the previous research focused on Permanent-Magnet Synchronous Motors (PMSMs), from §1.4 we can see that the PMSM and the SynRM share the same stator structure, so the acoustic noise calculation procedure in previous research can be repeated in this thesis. To conclude, loudness is a function of the natural mode frequency of the stator, the electromagnetic force wave and other parameters such as pole number, stator mass, etc.

Meanwhile, the natural mode frequency of the stator is determined by the following geometric parameters: tooth-width, slot-depth, tooth-tip thickness, tang-angle and number of slots. Currently, there are two ways to obtain the natural mode frequency of the stator. The first method uses an analytical computation method [1] [2], however, it doesn't take into account the effect of variations of stator tooth geometries such as tooth tang angle, tooth tip thickness etc. An alternate approach applies using the Finite Element Analysis (FEA)-based structural analysis software, such as *Nastran* [14], which is time- consuming. In this research, a neural network (NN) prediction model is proposed. Generally, a NN prediction model means that a model with multiple inputs can have multiple outputs as the estimation values. It is trained by a large true dataset. Using the software *Nastran* [14] we have built a large dataset, then using a neural network, we have built a prediction model which can estimate the natural mode frequency with an acceptable relative error rate. This is one of two original contributions in this thesis.

This thesis follows the loudness calculation procedure used for PMSM, and applies it to the SynRM. The second original contribution is to apply the NN model to the loudness calculation procedure in single barrier SynRMs. Hence a prediction model for estimating the loudness in SynRMS can be obtained.

Chapter 2

Introduction to Generalized Regression Neural Networks

2.1 Artificial Neural Networks Theory

2.1.1 Brief Introduction of Artificial Neural Networks

Artificial Neural Networks (ANNs) are models which are inspired by biological neural networks (the central nervous systems such as the brain). They are used to approximate functions that can base on a large number of inputs. In general, ANNs are specified by: the Architecture, the Activity Rule and the Learning Rule [15].

The Architecture specifies the relationship between the variables and the network involved.

The Activity rule defines how the activities of the neurons change in response to each other. It depends on the weights (the parameters) in the networks.

The Learning rule defines how the weights of neural networks change with time. It usually depends on the activity of the neurons.

2.1.2 Neural Network Models

Generally, neural network models are considered as artificial neural networks (ANNs). Usually, these are mathematical models which define a function **f**: $\mathbf{X} \rightarrow \mathbf{Y}$, but models can be also associated with a learning algorithm or learning rule. The phrase"Artificial Neural Network Model" is a definition of a class of such functions (where members of the class are obtained by varying parameters, connection weights, or specifics of the architecture such as the number of neurons or their connectivity).

Network Function

"A Network" means the interconnections between the neurons in different layers of the system. Using a three layer system as an example, the first layer has input neurons that can send data via synapses to the second layer of neurons and then via more synapses to the third layer, the output layer. There will be more layers of neurons when the systems are more complex. The synapses that store parameters are called "weights" and can manipulate the data in calculations.

2.1.3 Learning Algorithms of Neural Networks

The most interesting thing in neural networks is learning. When we are given a task to solve, for a class of functions F learning means utilizing a set of observations to find $f \in F$ such that the task can be solved.

There are several algorithms which can be used for training ANN models; most of them can be considered as the application of optimization theory and statistical estimation.

Backpropagation Methods, Evolutionary methods [16], gene expression programming [17], simulated annealing [18], expectation-maximization, non-parametric methods and particle swarm optimization [19] are some methods used for training neural networks.

2.2 Generalized Regression Neural Networks

2.2.1 Brief Introduction of GRNN

In 1991, Specht proposed the Generalized Regression Neural Network (GRNN) [20]. The GRNN has been widely applied in signal image processing [21], structural analysis [22], system design [23], the financial area (predict the risk of stocks and rate of exchange) [24],and in bioengineering problems [25, 26].

Generally, NNs are trained to map from a specific input to a particular target output until the network output matches the target. Thus, the NN can learn the mapping. The learning ability of a NN depends on its architecture and applied algorithm used during the training. Commonly used neural networks are the Back Propagation Neural Network (BPNN) and the Radial Basis Neural Network (RBNN).

The Back Propagation Neural Network (BPNN) is one of the most widely applied neural network models. It is a multi-layer feedforward network which uses a sigmoid function as the activation function and is trained with the error back propagation algorithm. [27]

The Radial Basis Neural Network (RBNN) is a kind of artificial neural network which uses the radial basis function as an activation function. A radial basis function (RBF) is a real-valued function whose value depends only on the distance from the origin, so that $\phi(x, c) = \phi(||x - c||)$, any function ϕ that satisfies the property $\phi(x) = \phi(||x||)$ is a radial function. For the RBNN, the predicted result of the network is the linear combination of radial basis functions of the input and the neuron parameters.

In this thesis, the GRNN (General Regression Neural Network) is introduced to predict the results. A GRNN could be viewed as a variation of the RBNN, it does not demand the iterative training procedure used in BPNN. It estimates any arbitrary function between input and output vectors, drawing the function estimates directly from the training data. Additionally, it is consistent in that, as the size of the training set becomes large, the estimation error approaches zero.

2.2.2 Theory of the GRNN

The GRNN is a memory-based NN that supplies estimates of continuous variables and convergence to the underlying (linear or nonlinear) regression surface. Its principle advantages are fast learning and convergence to the optimal regression surface as the number of samples becomes very large. Actually, the GRNN is a method of regression which uses the probability density function (PDF). Thus the approach is not limited to any particular function and requires no prior knowledge

The GRNN estimates the joint PDF using nonparametric estimators to get the conditional PDF and then get the expected value as the predicted result of regression.

Assume that $f(x, y)$ is the known joint continuous probability density function of a vector random variable, x, and a scalar random variable, y. Let X be a particular measured value of the random variable x.The regression of y on X (also the conditional mean of y on X) is given by:

$$E[y|X] = \frac{\int_{-\infty}^{+\infty} y f(X, y) dy}{\int_{-\infty}^{+\infty} f(X, y) dy} \tag{2.1}$$

Since the density $f(x, y)$ is not known, it should be estimated from a sample of observations of x and y,

$$f(X, Y) = \frac{1}{(2\pi)^{(p+1)/2}\sigma^{p+1}n} \cdot \sum_{i=1}^{n} \exp[-\frac{(X - X_i)^T (X - X_i)}{2\sigma^2}] \exp[-\frac{(Y - Y_i)}{2\sigma^2}] \tag{2.2}$$

Here, Y is the target value of y when given observed value X. p is the dimension of the vector variable x. σ is the smoothing factor, it controls the shape of $f(X, Y)$, usually it has some experienced values. The method to obtain the optimal smoothing factor is shown in

§2.2.4. Define the scalar function D_i^2,

$$D_i^2 = (X - X_i)^T (X - X_i) \tag{2.3}$$

Integrating all the equations above, the conditional mean can be presented as the following:

$$Y(X) = \frac{\sum_{i=1}^{n} Y_i \exp(-\frac{D_i^2}{2\sigma^2})}{\sum_{i=1}^{n} \exp(-\frac{D_i^2}{2\sigma^2})} \tag{2.4}$$

2.2.3 Structure of GRNN

A GRNN is made up of four layers: input layer, pattern layer, summation layer and output layer. The number of input units in the input layer depends on the total number of the observation parameters, the vector X. The first layer is connected to the pattern layer and in this layer the $f(x, y)$ is determined. The pattern layer is connected to the summation layer. There are two different types of summations in the summation layer, which are a single division unit and summation unit. The summation and output layer together perform a normalization of the output set. In the training of the network, radial basis and linear activation functions are used in the pattern, the summation and the output layers. Each pattern layer unit is connected to the two neurons in the summation layer, the summation unit and the division unit. The summation unit computes the sum of weighted responses of the pattern layer. On the other hand, the division unit is used to calculate un-weighted outputs of the pattern neurons. The output layer merely divides the output of each summation unit by that of each division unit, yielding the predicted response to an unknown vector. Equation (2.4) can be rewritten as

$$Y(X) = \frac{\sum_{i=1}^{n} A_i \exp(-\frac{D_i^2}{2\sigma^2})}{\sum_{i=1}^{n} B_i \exp(-\frac{D_i^2}{2\sigma^2})} \tag{2.5}$$

Here the summation unit is actually the numerator of the equation (2.5), while the division unit is the denominator of the equation (2.5). The architecture for the GRNN is shown in Fig.2.1:

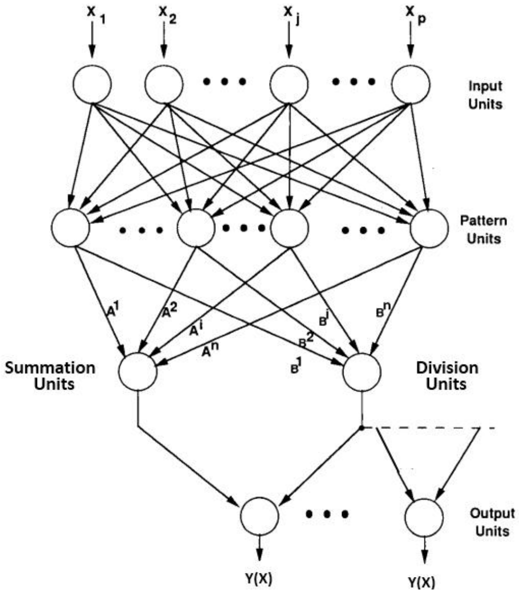

Fig. 2.1 GRNN Diagram [20]

2.2.4 Optimize Smoothing Factor

The $Y(X)$ can be viewed as a weighted average of all the Y_i, which are the observed values. Each observed value is weighted exponentially depend on its Euclidean distance from X. When the smoothing factor σ becomes large, the estimated density is made to be smooth and in the limit becomes a multivariate Gaussian with covariance σ_i^2. On the contrary, a smaller value of σ allows the estimated density to assume non-Gaussian shapes, but with the hazard that outliers may have a too great an effect on the estimate. As σ becomes very large, $Y(X)$ assumes the value of the sample mean of the observed Y_i, and as the σ goes to 0, $Y(X)$ assumes the value of the Y_i associated with the observation X. For intermediate values of σ, all Y_i are taken into consideration, but those which correspond to the points closer to X are given heavier weight.

When the underlying natural distribution is unknown, it is unable to determine an optimum σ for a given number of observations n. Hence, it is necessary to find σ on an empirical basis. This can be realized easily when the density estimate is being utilized in a regression equation, as there is an intuitive standard that can be utilized for evaluating each value of σ, namely, the mean square error between Y_j and the estimate $Y(X_j)$. [28] proposes a method to confirm the optimal value of the smoothing factor:

(1) Let the smoothing factor increase with a stepsize $\triangle\sigma$ in a specific range $(\sigma_{min}, \sigma_{max})$;

(2) Save one or two training samples, using the rest to train the neural network, then use the remaining samples to test the results;

(3) Use the network model to calculate the absolute value of the errors of the testing samples, known as the prediction error;

(4) Repeat (2),(3), until all the training samples have been used as test samples once, then calculate the average of the prediction error,

$$E = \frac{1}{n} \sum_{i=1}^{n} |Y_i - Y(X_i)| \tag{2.6}$$

2.2.5 Advantages of GRNN

Compared with BP-neural network, its highly parallel structure and the learning procedure makes it easily implemented on the hardware and removes the need for the time-consuming back propagation.

Compared to the radial basis neural network, it has a dynamic network structure. For some specific problems, the number of observations can be sufficiently large so that it is not practical to assign a separate unit to each sample. Various clustering techniques are used to find representative samples to reduce the size of the training set. Forgetting functions are taken into consideration to model a system with a changing characteristic and make it more robust to the outliers. The idea of a forgetting function is to decrease the effects of data which take only a small account. [20]

A GRNN is based on established statistical theories, and asymptotically converges with an increasing number of samples to the optimal regression surface, yielding better results than the BPNN or the RBNN.

Chapter 3

GRNN Prediction Model of Stator Natural Mode Frequency

3.1 Introduction of Stator Natural Mode Frequency

The magnetic radial force acting on the air gap between the rotor and stator can cause the deformation of the stator rings [2] [29]. Deformations of the stator core for different vibration modes are called ”mode shapes” [30]. The common vibration mode shapes can be seen in Fig.3.1 [30]

From the Fig.3.1, we can conclude that the mode number m actually represents the number of directions in which the magnetic forces act on the stator core. These modes can be excited simultaneously. Mode 0 means the stator is not acted on by a force, it’s what the undeformed stator looks like.

All the mode shapes have their own natural mode frequencies, each specific mode shape can be excited when its natural mode frequency matches one of the excitation frequencies of the magnetic radial force.

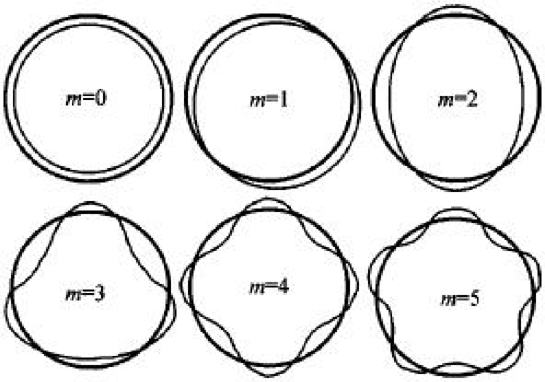

Fig. 3.1 Common Vibration Mode Shapes with mode number m [30]

3.2 Parameter Introduction

In this thesis, we use a 33 slot 8 pole SynRM as the example. Its cross-section surface is shown in the Fig.3.2. The main parts we need to consider in the stator are the tooth and

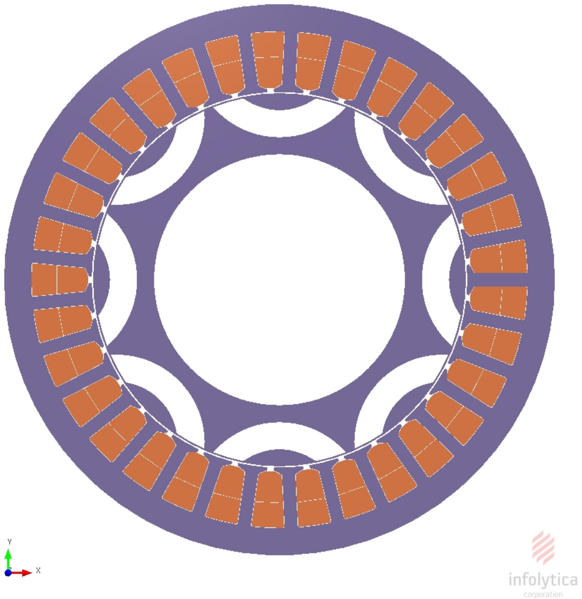

Fig. 3.2 Cross-section Surface of 33s8p SynRM

slot which are shown in Fig.3.3. The natural mode frequencies are functions of the stator geometry parameters [2]. Generally, each natural mode frequency corresponds to a unique vibration mode shape and once the vibration mode shape is defined, the natural mode frequency can be obtained. From Fig.3.2, Fig.3.3 and Fig.3.4 we can see that the tooth-width (a), slot-depth (b), tang-angle (c), tooth-tip thickness (d) and the number of slots (n) directly influence the stator shape. If these five parameters are fixed, the vibration mode shape is defined, hence the natural mode frequency can be determined. To conclude, let the natural mode frequency be y, the five parameters respectively are a, b, c, d, n, then there is a function which makes $y = f(a, b, c, d, n)$. As this function has never been given before, an approach to finding it is to train a prediction model which uses these five parameters as the inputs, and the natural mode frequency as the output.

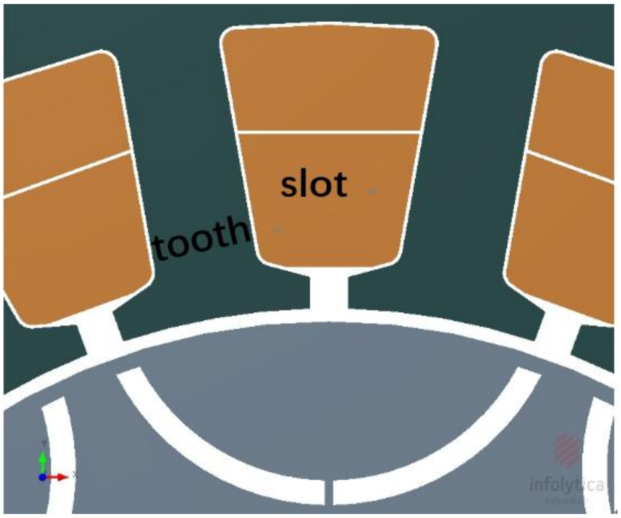

Fig. 3.3 Tooth and Slot

3.3 Prediction Results and Validation

Using the FEA-based software, *Nastran*, a large dataset was created to train our GRNN model. We assumed that the stator natural mode frequencies from FEA are relatively close

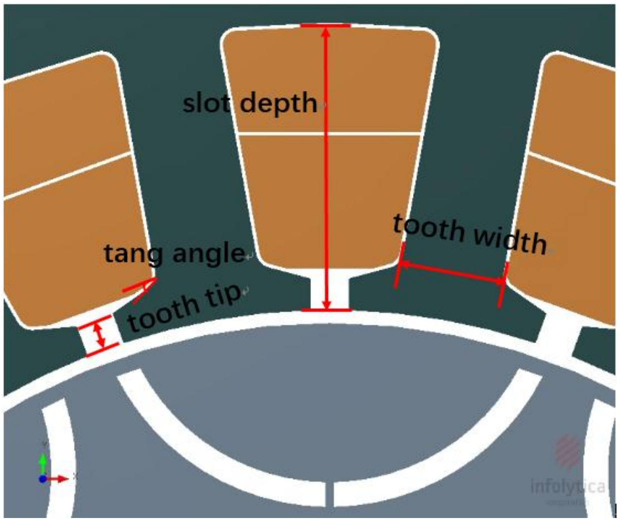

Fig. 3.4 Stator Geometry Parameters

to the true values in the real situation. The dataset includes the 9 slots, 12 slots, 15 slots, 18 slots, 21 slots, 24 slots, 27 slots, 30 slots and 33 slots' SynRM Stator models' natural mode frequencies which are from mode 1 to mode 10. Each kind of model has 882 specific models for various tooth-widths, slot-depths, tang-angles and tooth-tip thicknesses. For example, for Model No.1 in the 9 slots model, the geometry parameters are *tooth width: 34.2mm, slot depth: 36.65mm, tang-angle:* 20°*, tooth tip thickness: 2.96mm* , while the parameters for Model No.2 in the 9 slots model are *tooth width: 34.2mm, slot depth: 36.49mm, tang-angle:* 20°*, tooth tip thickness: 2.96mm.*

As explained in Chapter 2, the GRNN model has a smoothing factor. The value of the smoothing factor will influence the GRNN model prediction performance. Our strategy is to use the 9,12,15,18,21,24,27,30 slots' data combined with a smoothing factor to train the neural network prediction model, then use the cross validation method as explained in Chapter 2 to confirm the optimal smoothing factor. After that, using the prediction model to estimate the natural mode frequencies of the 33 slots stator and compare the values with the ones from the *FEA*.

As an example, some of the training samples of the 12 slots stator's natural mode frequencies are shown in Table.3.1.

Table 3.1 Part of the training samples of 12 slots stator natural mode frequencies from mode 1 to mode 5 (Hz)

Model Number	**Mode 1**	**Mode 2**	**Mode 3**	**Mode 4**	**Mode 5**
1	296.467	788.145	1366.065	2269.985	2886.011
5	311.116	825.435	1437.602	2375.465	3025.157
10	326.109	867.85	1509.44	2503.343	3187.927
15	348.312	927.661	1616.718	2667.862	3399.279
20	370.955	987.997	1725.165	2828.927	3588.933

The parameters of the samples are shown in Table.3.2 and.3.3. The reason why we show them in two tables is because, when constructing the training samples for the 1st half of the samples, we keep the tang-angle and tooth tip thickness as constant with different combinations of tooth width and slot depth, and for the 2nd half we keep the tooth width and slot depth as constant and vary the tang-angle and tooth tip thickness.

Table 3.2 Geometry Parameters of 1st Half Training Samples

Number of Slots	**Tooth Width (mm)**	**Slot Depth (mm)**	**Tang Angle (°)**	**Tooth Tip Thickness (mm)**
9	34.2∼41.8	33.35∼36.65	20	2.969
12	13.5∼16.5	29.5∼33.5	20	2.2
15	17.64∼21.56	24.44∼29.36	26	2.69
18	13.734∼16.786	25.914∼30.566	16	2.69
21	11.664∼14.256	27.014∼31.466	18	2.96
24	10.134∼12.386	30.314∼34.166	20	2.69
27	8.262∼10.098	31.7∼35.3	20	2.2
30	8.334∼10.186	32.91∼36.29	20	2.69

Table 3.3 Geometry Parameters of 2nd Half Training Samples

Number of Slots	Tooth Width (mm)	Slot Depth (mm)	Tang Angle (°)	Tooth Tip Thickness (mm)
9	38	35	18∼22	2.664∼3.256
12	25	35.7	18∼22	1.98∼2.42
15	19.6	26.9	23.4∼28.6	2.664∼3.256
18	15.26	28.24	14.4∼17.6	2.664∼3.256
21	12.96	29.24	16.2∼19.8	2.664∼3.256
24	11.26	32.24	18∼22	2.421∼2.959
27	9.18	33.5	18∼22	1.98∼2.42
30	9.26	34.6	18∼22	2.421∼2.959

3.3.1 Cross-Validation

For training the prediction model, not only do we need the training dataset, but also we need to pick a smoothing factor. Generally, there are four experience values, 0.3,0.5,0.7 and 1.0, which can be chosen as the alternative smoothing factor [20]. Then cross validation is used to confirm the optimal smoothing factor. For our training dataset, we randomize the dataset first, then divide it into nine parts. (This is still a Leave-One-Out approach. We break the set into 9 parts and then use one of the parts as a cross-validation set while the rest of the parts as the training sets, until all the parts have been used as the cross-validation set. Usually, for a large dataset, we divide it into 10 folds doing the cross-validation to save the computation time. Here, the size of the dataset is 882 multiplied by 8 models, 9 is the number that the dataset can be divided evenly.) Each time we use eight parts to train the model and use the model we obtain to predict the values of the remaining part's outputs. Finally we compute the *Root Mean Square Relative Error*(RMSRE). Hence, for each prediction model, we get a 9×10 RMSRE matrix. 9 is the number of the times of the validation, 10 is the number of RMSRE corresponding to each natural mode frequency. For example, the element in the 3rd row 1st column is the RMSRE of mode 1 for the 3rd time cross-validation. The RMSRE function is shown in equation (3.1):

$$RMSRE = |\sqrt{\frac{\sum_{i=1}^{n}(f_{p_i} - f_{m_i})/f_{m_i}}{n}}| \times 100\% \tag{3.1}$$

f_{p_i} is the prediction value of the natural mode frequency of the ith model, while f_{m_i} is the “accurate” value from FEA. Here $n = 784$ which is one ninth of the training samples. Part of the cross-validation results, which are from mode 1 to mode 5, can be seen in Table.3.4, Table.3.5, Table.3.6 and Table.3.7.

Table 3.4 Cross Validation Results Of the Prediction Model with the Smoothing Factor 0.3

	Mode 1	**Mode 2**	**Mode 3**	**Mode 4**	**Mode 5**
validation1	0.33%	0.33%	0.33%	0.33%	0.29%
validation2	0.42%	0.42%	0.43%	0.43%	0.38%
validation3	0.31%	0.31%	0.32%	0.32%	0.29%
validation4	0.37%	0.37%	0.37%	0.37%	0.37%
validation5	0.38%	0.38%	0.39%	0.37%	0.32%
validation6	0.38%	0.39%	0.39%	0.38%	0.33%
validation7	0.30%	0.31%	0.31%	0.31%	0.28%
validation8	0.34%	0.35%	0.35%	0.34%	0.31%
validation9	0.34%	0.34%	0.35%	0.35%	0.33%

It can be seen from the cross validation tables that the neural network model with a smoothing factor 0.3 has the lowest RMSRE. So in this case, we have assumed that smoothing factor 0.3 is optimal.

Table 3.5 Cross Validation Results Of the Prediction Model with the Smoothing Factor 0.5

	Mode 1	**Mode 2**	**Mode 3**	**Mode 4**	**Mode 5**
validation1	0.69%	0.69%	0.70%	0.69%	0.62%
validation2	0.76%	0.76%	0.78%	0.74%	0.66%
validation3	0.68%	0.68%	0.69%	0.67%	0.58%
validation4	0.71%	0.71%	0.71%	0.71%	0.61%
validation5	0.69%	0.69%	0.70%	0.68%	0.58%
validation6	0.65%	0.66%	0.66%	0.65%	0.61%
validation7	0.73%	0.74%	0.75%	0.74%	0.67%
validation8	0.69%	0.70%	0.71%	0.71%	0.63%
validation9	0.65%	0.65%	0.66%	0.65%	0.60%

Table 3.6 Cross Validation Results Of the Prediction Model with the Smoothing Factor 0.7

	Mode 1	**Mode 2**	**Mode 3**	**Mode 4**	**Mode 5**
validation1	1.24%	1.25%	1.25%	1.22%	1.06%
validation2	1.24%	1.26%	1.26%	1.24%	1.07%
validation3	1.22%	1.23%	1.24%	1.21%	1.06%
validation4	1.19%	1.20%	1.21%	1.19%	1.07%
validation5	1.27%	1.29%	1.30%	1.28%	1.13%
validation6	1.19%	1.20%	1.21%	1.18%	1.02%
validation7	1.26%	1.27%	1.28%	1.27%	1.12%
validation8	1.18%	1.20%	1.20%	1.17%	1.01%
validation9	1.13%	1.15%	1.15%	1.14%	1.00%

Table 3.7 Cross Validation Results Of the Prediction Model with the Smoothing Factor 1.0

	Mode 1	**Mode 2**	**Mode 3**	**Mode 4**	**Mode 5**
validation1	1.24%	1.25%	1.25%	1.22%	1.06%
validation2	1.24%	1.24%	1.26%	1.24%	1.07%
validation3	1.22%	1.23%	1.24%	1.21%	1.06%
validation4	1.09%	1.20%	1.21%	1.19%	1.07%
validation5	1.27%	1.29%	1.30%	1.28%	1.13%
validation6	1.19%	1.20%	1.21%	1.18%	1.02%
validation7	1.26%	1.27%	1.28%	1.27%	1.12%
validation8	1.18%	1.20%	1.20%	1.18%	1.01%
validation9	1.13%	1.15%	1.15%	1.14%	1.00%

3.3.2 Test With 33 Slots' Data

As we explained before, for the first half of models from *FEA*, the tang angle and tooth tip thickness were kept constant, for the second half, the tooth width and slot depth were kept constant. The geometric parameters of the 33 slots stator are shown in Table.3.8. Using the neural network model which was trained on 9,12,15,18,21,24,27 and 30 slots example, the accuracy is tested by comparing the prediction value and the FEA value of the natural mode frequency of the 33 slots stator. The relative error is designed to show how close the

Table 3.8 Geometry Parameters of 33 Slots' Stator

	1st Half	**2nd Half**
Tooth Width (mm)	6.966∼8.514	7.74
Slot Depth (mm)	34.23∼37.37	35.8
Tang Angle (°)	25	22.5∼27.5
Tooth Tip Thickness (mm)	1.58	1.422∼1.738

prediction value is to the FEA value. The function for the relative error of the jth mode of the ith model is shown below:

$$Error_{Relative} = |\frac{f_{p_{ij}} - f_{m_{ij}}}{f_{m_{ij}}}| \times 100\% \tag{3.2}$$

Here $f_{p_{ij}}$ is the prediction value of the jth mode of ith model's frequency, while $f_{m_{ij}}$ is the FEA value.

As there are 882 samples and each sample has 10 mode frequencies, there are 8820 relative error results in total. Some of the model's relative errors from mode 1 to mode 5 are listed in Table.3.9

Table 3.9 Part of the Relative Error of 33 slots stator

Model No.	**Mode 1**	**Mode 2**	**Mode 3**	**Mode 4**	**Mode 5**
10	6.86%	7.46%	8.72%	11.96%	18.54%
100	3.22%	3.48%	4.37%	6.85%	11.97%
200	7.71%	8.36%	9.07%	11.11%	15.09%
300	14.80%	15.56%	16.30%	17.75%	20.06%
400	24.22%	25.32%	25.89%	27.17%	28.83%
500	7.77%	8.41%	9.08%	11.02%	14.69%
600	7.80%	8.47%	9.16%	11.08%	14.73%
700	7.84%	8.49%	9.20%	11.10%	14.77%
800	7.85%	8.54%	9.20%	11.12%	14.83%

Table.3.10 shows the range of the relative error from the 882 samples under each mode of the 33 slot stator.

Morover, we use the neural network model which was trained with 7 slot numbers (9, 12, 15, 18, 21, 24, 27) to determine the prediction accuracy for the 33 slot stator if there are fewer training samples. Some of the model's relative errors from mode 1 to mode 5 are

Table 3.10 Range of the Relative Error of 33 slots stator

	Maximum	**Minimum**	**Average**
Mode1	24.41%	0.03%	8.62%
Mode2	25.48%	0.0004%	9.21%
Mode3	26.00%	0.02%	9.88%
Mode4	27.21%	0.30%	11.76%
Mode5	33.31%	2.39%	15.54%

listed in Table.3.11

Table 3.11 Part of the Relative Error of 33 slots stator (trained by 7 slot numbers)

Model No.	**Mode 1**	**Mode 2**	**Mode 3**	**Mode 4**	**Mode 5**
10	15.79%	16.22%	16.87%	18.91%	22.96%
100	11.85%	11.91%	12.19%	13.48%	16.14%
200	16.72%	17.19%	7.25%	18.01%	19.38%
300	24.39%	24.98%	25.02%	25.05%	24.54%
400	34.60%	35.53%	35.33%	35.07%	33.64%
500	16.77%	17.24%	17.25%	17.89%	18.95%
600	16.81%	17.32%	17.34%	17.98%	19.00%
700	16.86%	17.34%	17.40%	18.01%	19.06%
800	16.88%	17.40%	17.40%	18.04%	19.14%

Table.3.12 shows the range of the relative errors from the 882 samples under each mode of the 33 slot stator which are predicted by the neural network trained by 7 different slot numbers.

Fig.3.5 and Fig.3.6 illustrate the comparison of the relative error of mode 1 and mode 3 from two different neural network models trained by training set (P) and training set (P*).

Table 3.12 Range of the Relative Error of 33 slots stator (trained by 7 slot numbers)

	Maximum	**Minimum**	**Average**
Mode1	34.81%	3.63%	17.17%
Mode2	35.71%	3.85%	17.62%
Mode3	35.44%	3.33%	17.69%
Mode4	35.10%	2.82%	18.35%
Mode5	38.28%	1.85%	19.45%

The triangle (P) training set given the natural frequencies for stator cores ranging from 9 to 30 slots (8 different slot number) while the squares (P*) correspond to those between 9 and 27 (7 different slot number) slots. Clearly, the results using training set P are better than those using P*. From the tables above and Fig.3.5 Fig.3.6, we can see clearly that more training samples, the more accurate the prediction model will be. Also, the GRNN prediction model can estimate the natural mode frequencies of the stator well if given a large training set.

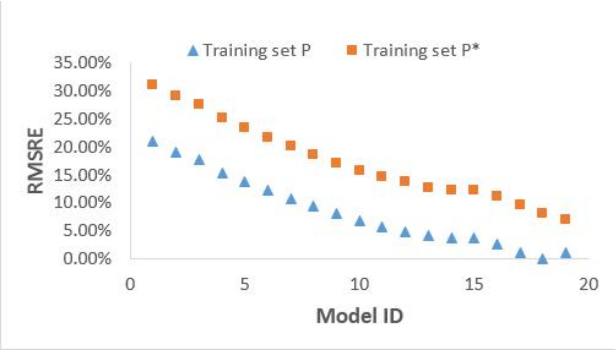

Fig. 3.5 Mode 1 error Comparison between NN model from two training set

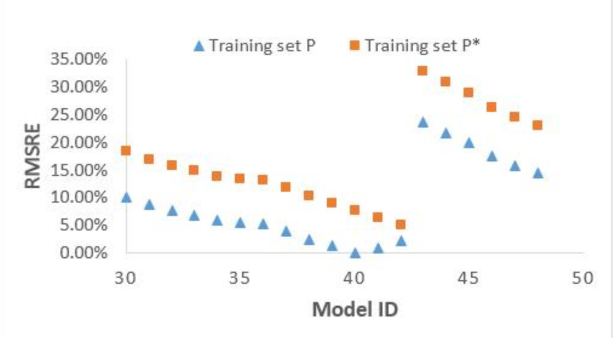

Fig. 3.6 Mode 3 error Comparison between NN model from two training set

3.4 Summary

In this chapter, we proposed our GRNN prediction model for estimating the natural mode frequencies of the stator. The model was trained by using 8 different slot numbers (9, 12, 15, 18, 21, 24, 27, 30), and 4 different smoothing factors (0.3, 0.5, 0.7 and 1.0) were used in training. Using the cross-validation method, we affirmed that 0.3 is the optimal smoothing factor, so the GRNN model finally chosen is the one trained with 8 different slot number with the smoothing factor 0.3. Once the prediction model was obtained, it was tested with the 33 slot data and then the values both from our GRNN model and the values from *FEA* were compared to compute the relative error.

We also computed the relative error resulting from the GRNN models trained with different training samples, the results show that if there are more training sets, the GRNN model will be more accurate.

Moreover, it seems that the prediction results have an error around 15% which is bigger than the cross-validation results. Predicting the test data of slot 33 is performing an extrapolation of the dataset (only has the slot 9/12/15/18/21/24/27/30). This may be one explanation of the error. An alternate test would be to include the 33 slots data in the training set and then leave out an alternate set of data, e.g. slot 18, and test the network prediction for this data. Another possibility is that the data has been over-fitted by the network. Further tests are needed to determine which of these is the reason of the error.

Chapter 4

Loudness Calculation

In the last chapter, we built a GRNN prediction model for estimating the value of the stator's natural mode frequencies. In this chapter, we are going to use them to implement the loudness calculation.

Looking back at the principle of how acoustic noise is generated in motors, there are three sources which are *aerodynamic*,*mechanical* and *electromagnetic*. As the electromagnetic source is the dominant one, we are only discussing the noise with an electromagnetic origin in this thesis. This is a result of the radial magnetic force due to the magnetic flux density waveforms in the air gap between the stator and the rotor [2] [6].

The strategy is that we calculate the pressure wave in the air gap so that the radial forces can be determined, then combining it with the natural mode frequencies of the stator, the radial displacements in the stator can be determined. Using the radial displacements we can calculate the total sound pressure level which can help us estimate the loudness value. In this case, the loudness value is a function of radial displacements, and these are functions of natural mode frequencies. We can utilize our GRNN model to predict the values of the radial displacements and thus predict the values of the loudness. The diagram of this strategy is shown in Fig.4.1

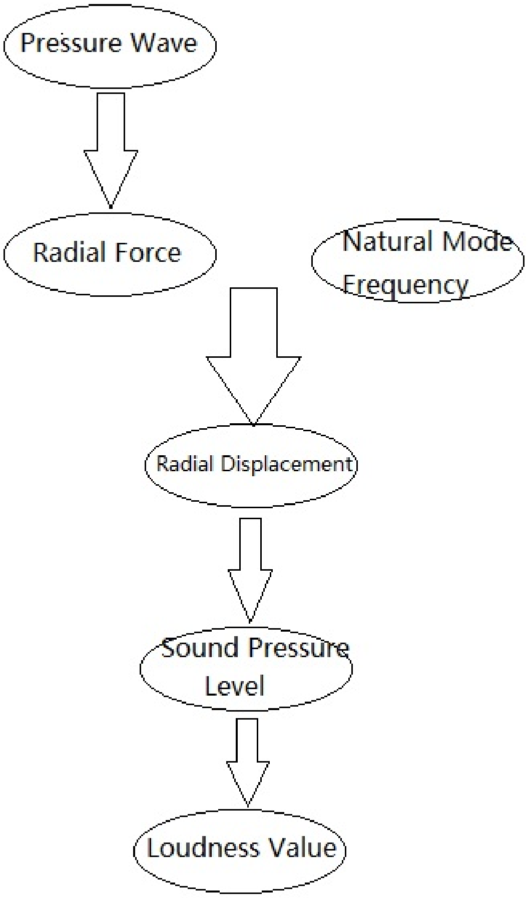

Fig. 4.1 Strategy Diagram

4.1 Pressure Wave in The Air Gap

The force in the air gap can be divided into F_{rad} which is in the radial direction and F_{tan} which is in the tangential direction. They are shown in the Fig.4.2.

The forces can be calculated by the equations given in [1]

$$F_{tan} = \frac{L_{stk}}{\mu_0} \oint_l B_t B_r dl \tag{4.1}$$

$$F_{rad} = \frac{L_{stk}}{2\mu_0} \oint_l B_r^2 - B_t^2 dl \tag{4.2}$$

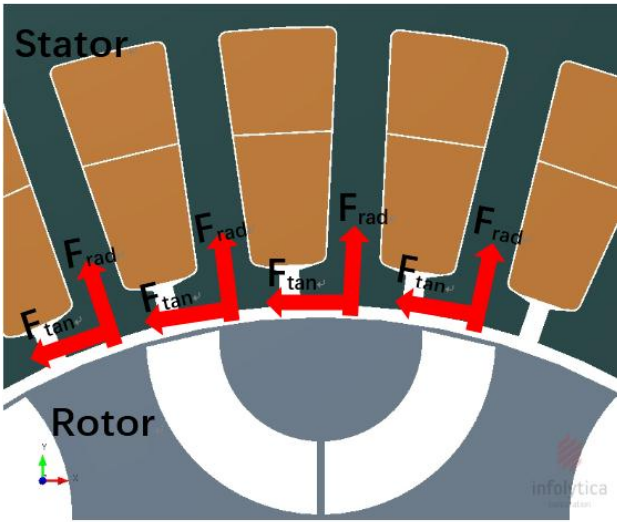

Fig. 4.2 Radial and tangential components of electromagnetic forces

Here, B_t and B_r represent the tangential and radial components of the flux density in the air gap, while L_{stk} is the stack length of the motor and l is the length of a line in the airgap that encloses the contour that the force acts on. $\mu_0 = 0.4\pi \times 10^{-6} H/m$ is the magnetic permeability of free space. As we know that the magnetic permeability of the ferromagnetic core is much higher than that of the air gap, the magnetic flux lines are actually perpendicular to the stator and rotor surface. Thus we can conclude that the radial component of flux is much larger than the tangential component, which means that the tangential component can be neglected. Another thing we need to emphasize is that the force per unit area is pressure. So for the value of radial pressure is as shown in the equation (4.3), the unit is $Pascal$

$$P_r(\alpha) \approx \frac{F_{rad}}{L_{stk}.l} = \frac{B_r^2(\alpha)}{2\mu_0} \tag{4.3}$$

4.1.1 Flux Carrier and Flux Barrier of Rotor

The value of the flux density in the air gap is influenced by two main electromagnetic components per rotor pole: the *flux barrier* and the *flux carrier*. Changing the width of the *flux barrier* and the *flux carrier* can change the value of the flux density in the air gap. Fig.4.3 shows these two parameters in the 8 pole case. A *flux barrier* consists of a non-ferromagnetic material leading to a high magnetic reluctance path, while the *flux carrier* is the opposite case.

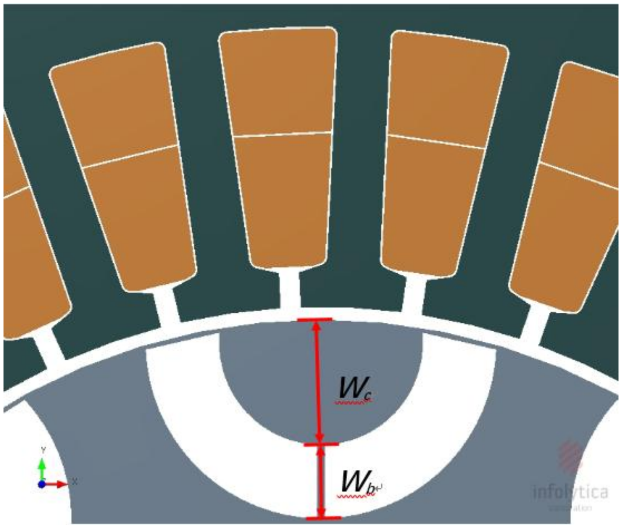

Fig. 4.3 Width of the flux barrier and flux carrier in an 8pole SynRM rotor [31]

Using the same stator configuration, we vary the width of the *flux barrier* and the *flux carrier* to get different rotor structures so that we can get different distributions of flux density in the air gap. We have designed 90 SynRM models which have the same stator configuration with different rotor structures. Finally, we will compute the loudness level of these 90 models.

4.1.2 Value of Flux Density in The Air Gap

The value of the flux density in the air gap is a periodic function of the angle α in the air gap.

Using the software *MagNet* [32] we obtained 2000 values for each model over a period which correspond to the position from $\alpha = 0$ to $\alpha = 360°$ in the air gap. Table. 4.1 shows part of the example models' (8poles 33slots) partial air gap flux density when the current level is 100%. The unit of the flux density is $Tesla(T)$.

Table 4.1 Part of the models (8poles 33slots) partial air gap flux density (T) with 100% current level

Model ID	Wc (mm)	Wb (mm)	0°	36°	72°	180 °	270°	324°	360°
15	18	2	0.86	0.88	0.84	0.24	0.78	0.64	0.86
30	12	14	0.72	0.74	0.72	0.04	0.49	1.19	0.72
45	10	2	0.78	0.75	1.18	0.15	0.59	1.02	0.78
60	6	14	0.54	0.58	1.09	0.00	0.17	0.36	0.54
75	4	8	0.53	0.34	1.36	0.02	0.17	0.52	0.53
90	2	4	0.61	0.65	1.01	0.06	0.48	0.50	0.61

Note that the value of flux density of model No.60 at 180° is actually $0.0004T$.

4.1.3 Harmonics of the Pressure Wave

Using the equation (4.3), we can acquire the radial component of the pressure values $P(\alpha)$ for each mechanical angle α. Table.4.2 shows part of the models' partial air gap pressure wave. The unit of the pressure wave is $Pascal(Pa)$.

In order to determine the amplitude of the radial displacement of the stator, we need to obtain the force which acts on the whole area of the inner surface of the stator. Only the value of the pressure wave at each angle is not enough, it is necessary to acquire the

Table 4.2 Part of the models partial air gap pressure wave (Pa)

Model ID	0°	36°	72°	180 °	270°	324°	360°
15	294869.10	307485.60	177108.30	23611.54	240979.30	165469.40	294869.10
30	208564.80	216818.90	130894.00	712.93	97215.78	592606.80	208564.80
45	240008.90	222269.40	318719.60	9418.55	138253.50	466664.60	240008.90
60	114580.70	134031.30	422740.80	0.07	11783.06	65823.08	114580.70
75	113589.60	44759.85	422412.40	113.15	11284.99	106968.90	113589.60
90	146679.60	1666609.00	235548.20	1211.11	90163.50	103383.20	146679.60

pressure wave which acts on the whole area. In this case, we determine the harmonics of the pressure wave from its *Fourier Series* which is based on an assumption that every periodic function can be represented by a sum of a (possibly infinite) set of simple oscillating functions, namely sines and cosines (or, equivalently, complex exponentials). Here, for the radial pressure wave P_r its real components of the *Fourier Series* can be represented as:

$$P_r(\alpha) = \sum P_{r_n} cos(w_n \alpha + ph_n) \tag{4.4}$$

Where P_{r_n} is the amplitude of the n_{th} order harmonic pressure wave. w_n is its frequency, and ph_n is the phase, the unit is $radian(rad)$.

Table.4.3 show part of our example model's (Model No.1 in 8 pole 33 slots) parameter values of the harmonic pressure wave.

The excitation frequency (f_e) of each harmonic is an integer multiple of the machine rotational frequency (f_p) which is given by [33]:

$$f_e(n) = n * f_p = n * \frac{w_r N_p}{120} \qquad n = 1, 2, 3 \cdots \tag{4.5}$$

Where n is the number of the harmonic order, w_r is the rotor rotational speed with the

Table 4.3 Part of the example models partial air gap pressure wave harmonic parameters

Harmonic Order **Parameters**	**1**	**5**	**10**	**25**	**50**	**100**
$P_r(Pa)$	35777.30	5827.75	11028.55	69059.00	6212.96	783.90
$w(Hz)$	0.16	0.80	1.60	3.98	7.96	15.92
$ph(rad)$	-1.94	0.63	-2.46	-1.56	2.88	-0.99

unit of rpm, N_p is the number of rotor poles. For instance, our example motor which is 8 poles 33 slots and has a rotational speed of 500 rpm, will have a rotational frequency $f_p = \frac{500 * 8}{120} = 33.33$Hz. Table.4.4 and Table.4.5 show part of the example models' (8poles 33slots) partial pressure wave harmonics amplitude, and their corresponding excitation frequencies when the rotational speed is 500 rpm. The unit of the harmonic pressure wave is $Pascal(Pa)$. Fig.4.4 shows the harmonic amplitude spectrum of the Model No.1 of the 8 poles 33 slots motor.

Table 4.4 Part of the example models partial air gap pressure wave amplitude (Pa)

Harmonic Order **Model ID**	**1**	**5**	**10**	**25**	**50**	**100**
15	23522.33	4567.261	3664.807	79464.78	5777.191	4110.326
30	30998.35	5684.859	2521.488	59232.85	3005.929	4340.038
45	5882.313	3023.792	2991.961	57804.03	4618.66	2677.021
60	22007.58	6230.527	2981.778	69547.56	911.6741	2223.278
75	27956.87	4679.431	5198.736	63597.08	3073.733	2161.219
90	19278.27	3331.333	3122.424	55606.9	4737.735	4121.483

Table 4.5 Part of the harmonics excitation frequency (Hz)

Harmonic Order	**1**	**5**	**10**	**25**	**50**	**100**
Excitation Frequency (Hz)	33.33	166.67	333.33	833.33	1666.67	3333.33

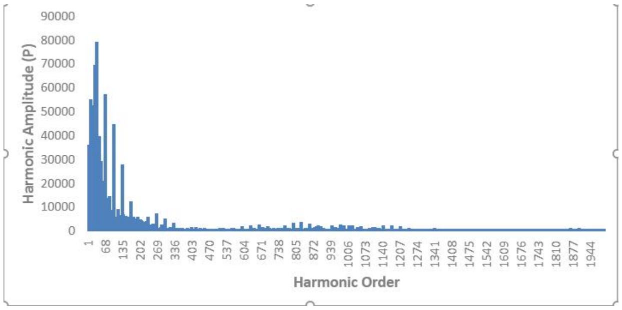

Fig. 4.4 Harmonic Amplitude Spectrum of the Example Model

4.2 Amplitude of The Radial Displacement of Stator

Since the harmonics of the pressure wave in the air gap have been obtained, we can determine the radial displacement of the stator under each mode by the approach detailed below.

4.2.1 Calculation Procedure

Again, the reason why we need to obtain the Fourier Series of the pressure wave in the air gap is because we need to determine the pressure wave which acts on the whole area of the inner surface of the cylindrical frame, so that the radial force can be determined. The Fourier Series of the radial pressure wave (P_r) has been shown in the equation (4.4). The P_r in the air gap can be viewed as the sum of the harmonic pressure waves, and each of those can be seen as a single pressure wave which acts on the whole area. As we mentioned before, the P_r is a periodic function of the angle α in the air gap from 0 to 2π. P_{r_n} is the amplitude of the n_{th} harmonic pressure wave. The radial force per unit area is the pressure wave, so it can be obtained from the integration of the harmonic pressure wave over the area of the inner surface of the cylindrical frame.

Note that the inner surface of the cylindrical frame S_i can be determined by equation

(4.6) where R_i is the inner radius of the stator; L_f is the stack length of the stator.

$$S_i = 2\pi * R_i * L_f \tag{4.6}$$

We can determine the n th order harmonic radial force F_{r_n} in the air gap by the equation (4.7), where l is the arc length, and $\frac{l}{R_i}$ is the angle corresponding to the arc length, dl_f is the differential of the stack length, P_{r_n} is the amplitude of the nth harmonic pressure wave.

$$F_{r_n} = \int_0^{L_f} \int_0^{2\pi R_i} P_{r_n} * cos(w_n \frac{l}{R_i} + ph_n) dl dl_f \tag{4.7}$$

Equation (4.7) can be rewritten as

$$F_{r_n} = \int_0^{2\pi} P_{r_n} * cos(w_n \alpha + ph_n) d\alpha * R_i * L_f \tag{4.8}$$

From Fig.4.4 we can see that the first 50 harmonics are the dominant ones. In order to save the computation time we only use first 50 harmonics.

Each harmonic force will excite all the 10 mode shapes, while the displacement of the i_{th} mode shape excited by the n_{th} order harmonic can be calculated by the equation (4.9) [1] [6]

$$A_{i_n} = \frac{F_{r_n}/[(2\pi f_{m_i})^2 M]}{\sqrt{[1 - (f_{e_n}/f_{m_i})^2]^2 + [2\zeta_i (f_{e_n}/f_{m_i})]^2}} \tag{4.9}$$

Where f_{e_n} is the excitation frequency of the n_{th} order harmonic, f_{m_i} is the stator i_{th} natural mode frequency, and i is in the range from 1 to 10. M is the mass of the stator. ζ_i is the damping ratio of the i_{th} mode which also affects the computation and can be determined by equation (4.10) [34]. In engineering, the damping ratio is a measure describing how oscillations in a system decay after a disturbance. The damping ratio is a measure of describing how rapidly the oscillations decay from one bounce to the next.

$$\zeta_i = \frac{1}{2\pi}(2.76 \times 10^{-5} f_{m_i} + 0.062) \tag{4.10}$$

Equation (4.9) also explains the principle of resonance that the amplitude of the displacement is actually influenced by the magnitude of the exterior force, which is F_{r_n} in the equation and the closeness of f_{e_n} and f_{m_i}. Suppose that if f_{e_n} is equal to f_{m_i}, then the denominator of this equation will be the minimum value, and the amplitude will be big.

As i is from 1 to 10, there will be 10 values of ζ_i which correspond to 10 stator natural modes. So the results of A_{i_n} will be a 10×50 matrix, each entry in the matrix represents a displacement of a specific mode shape under each harmonic's excitation. Then we can obtain A_i which is the total displacement of a specific mode. For a given motor example, there will be 10 A_i values which can be calculated by equation (4.11)

$$A_i = \sum_n A_{i_n} \tag{4.11}$$

4.2.2 Results

In this Chapter, we are using an 8 pole 33 slots SynRM as our example motor to show the calculation procedure. For the loudness calculation, the configuration of the stator is the same for all the example motors. The only difference is that we are changing the carrier width and barrier width of the rotor part as we explained previously in this chapter.

The geometry parameters of the stator are listed in Table.4.6

We use two sets of the mode frequencies to compute the displacement, one is from the *FEA* and we assume these mode frequencies are closer to the accurate values, the other comes from the GRNN prediction model as we explained in Chapter 3. These two groups of mode frequencies are listed in Table.4.7

Obviously, a different set of mode frequencies will determine a different value of the

Table 4.6 Geometry parameters of the example motor stator

Number of slots	33
Tooth Width (mm)	7.74
Slot Depth (mm)	35.8
Tang Angle (°)	25
Tooth Tip Thickness (mm)	1.58

mode displacement. Table 4.8 and Table 4.9 show part of the example motor's mode displacement in (μm) calculated with the mode frequencies from the FEA and GRNN prediction models.

Both of the results show that, as the mode number increases, the displacement will decrease. It can be seen that the first several modes have the most significant displacements which show that they are the dominant modes.

4.3 Sound Pressure Level

We will determine the sound pressure level of each mode by the mode displacement.

4.3.1 Calculation Procedure

The unit of *Sound Pressure Level* (SPL) is $Pascal(Pa)$, and SPL_i, which is SPL of each mode, can be calculated by equation (4.12)

$$SPL_i = 2\pi\rho c f A_i \tag{4.12}$$

Where ρ is the air density with the unit kg/m^3, c is the speed of sound, i.e. $344m/s$, f is the frequency of the displacement in Hz, from [5], we can find that the frequency of the displacement depends on the pole number. For a 4 pole motor, the $f = 4$, for an 8 pole

Table 4.7 Natural mode frequencies of the example motor (Hz)

	FEA Value	**Prediction Value**
Mode 1	317.389	342.375
Mode 2	850.174	922.971
Mode 3	1527.159	1668.301
Mode 4	2237.617	2487.711
Mode 5	2836.391	3258.907
Mode 6	3241.721	3807.919
Mode 7	3482.444	3868.841
Mode 8	3628.727	4282.128
Mode 9	3717.019	4529.449
Mode 10	3732.205	4692.866

motor, the $f = 8$ and for a 10 pole motor, $f = 10$. As we've determined the SPL_i, the total SPL can is given by equation (4.13)

$$SPL = \sum_i SPL_i \tag{4.13}$$

4.3.2 Results

We also get two sets of SPL values which are from the two displacement sets. Table 4.10 shows part of the example model's SPL value (Pa) from different displacements.

4.4 Loudness Results

The loudness level (L_w) in dB can be acquired from the sound pressure level.

Table 4.8 Part of the example model's radial displacement calculated with mode frequencies from FEA (μm)

Model ID	**1**	**2**	**3**	**4**	**5**	**6**
Mode 1	135.92	60.05	141.16	23.99	36.10	101.27
Mode 2	141.06	10.90	145.35	26.56	39.83	104.93
Mode 3	34.31	26.67	35.39	17.44	30.56	34.78
Mode 4	34.02	26.69	34.99	17.74	30.17	34.28
Mode 5	13.37	11.29	12.05	8.63	9.61	10.48
Mode 6	13.29	11.23	11.96	8.58	9.52	10.40
Mode 7	5.28	4.47	5.07	3.73	4.32	4.69
Mode 8	5.27	4.46	5.07	3.72	4.31	4.68
Mode 9	3.24	2.75	3.14	2.31	2.69	2.92
Mode 10	3.23	2.74	3.13	2.30	2.68	2.90

4.4.1 Calculation Procedure

L_w can be calculated by equation (4.14), which is also the loudness definition equation.

$$L_w = 10\log_{10}(\frac{SPL}{SPL_{ref}}) \tag{4.14}$$

Where the reference sound pressure level (SPL_{ref}) is $2 \times 10^{-5} Pa$.

4.4.2 Results

Table 4.11 shows part of the example models loudness level from the two different sources of mode frequency

Table 4.9 Part of the example model's radial displacement calculated with mode frequencies from the Prediction Model (μm)

Model ID	**1**	**2**	**3**	**4**	**5**	**6**
Mode 1	226.47	103.88	211.61	74.26	108.72	166.77
Mode 2	30.00	24.87	30.21	18.39	25.75	28.95
Mode 3	10.65	9.19	9.51	7.07	7.48	8.27
Mode 4	4.24	3.59	4.09	3.01	3.49	3.79
Mode 5	2.45	2.08	2.38	1.75	2.04	2.21
Mode 6	1.79	1.52	1.74	1.28	1.49	1.62
Mode 7	1.73	1.47	1.68	1.24	1.45	1.57
Mode 8	1.41	1.20	1.37	1.01	1.18	1.28
Mode 9	1.26	1.07	1.23	0.91	1.06	1.14
Mode 10	1.18	1.00	1.14	0.84	0.98	1.06

4.5 More Results and Discussion

In the last section, we used the 8 poles 33 slots model when the current level is 100% to show the loudness calculation procedure. In this section, more results will be shown to discuss how the current level and slot number influence the loudness.

4.5.1 Current level influence

Fig.4.5, Fig.4.6 and Fig.4.7 show the loudness prediction results of the 4 poles 15 slots, 8 poles 33 slots and 10 poles 27 slots models when working at three current levels. The circles, triangles and squares represent the loudness results when the models work at 50%, 100% and 200% current level respectively.

We can see clearly in the figure that each model has the highest loudness level when the current level is at the 200% current level, and when the current level is at the 50%, the

Table 4.10 Part of the example model's SPL (Pa)

Model No.	FEA	Prediction
1	7.99	5.78
2	2.20	3.08
3	8.16	5.44
4	2.36	2.25
5	3.48	3.16
6	6.40	4.45

Table 4.11 Part of the example model's loudness level (dB)

Model No.	FEA	Prediction
1	56.02	54.61
2	50.42	51.87
3	56.11	54.35
4	50.72	50.52
5	52.42	51.98
6	55.05	53.47

loudness level is the lowest. The results show that the loudness generally increases with increasing current level. Similar conclusions also apply for other models.

4.5.2 Slot number influence

A series of example models also have been designed to see the effects of changing the number of slots at a fixed pole number and for variable rotor configurations. They are 4 poles 15 slots and 24 slots; 8 poles 9 slots and 27 slots; 10 poles 12 slots and 33 slots. The loudness prediction results for them are shown below, here the triangles are the SynRMs with lower slot number and the circles are the ones with higher slot number.

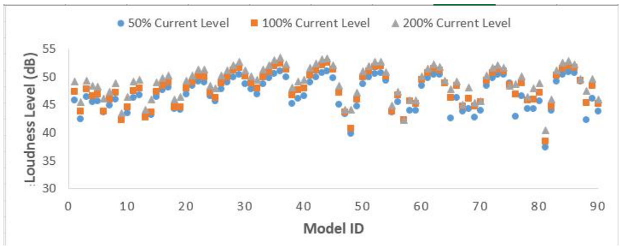

Fig. 4.5 4 poles 15 slots three current level loudness results

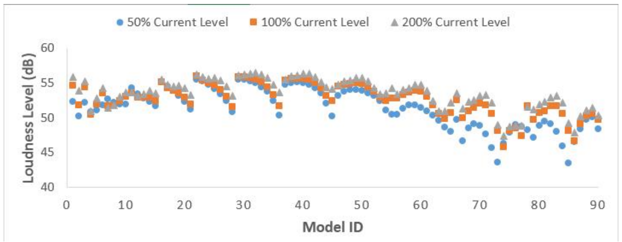

Fig. 4.6 8 poles 33 slots three current level loudness results

The results show that the loudness generally increases with the lower slot numbers if the rotor configurations are kept constant.

4.6 Summary

In this chapter, we have introduced an analytical method for calculating the noise level of the SynRM. Not only did we use the mode frequencies which come from FEA, but also the mode frequencies from the GRNN prediction model are also applied in our experiment. We use the 8 poles 33 slots models as the examples to follow the calculation procedure. The

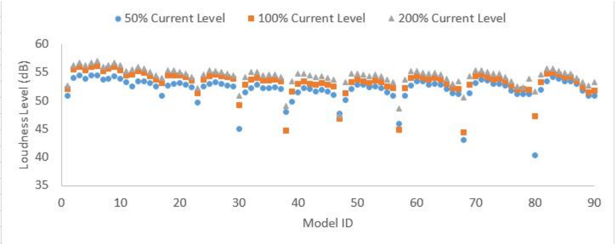

Fig. 4.7 10 poles 27 slots three current level loudness results

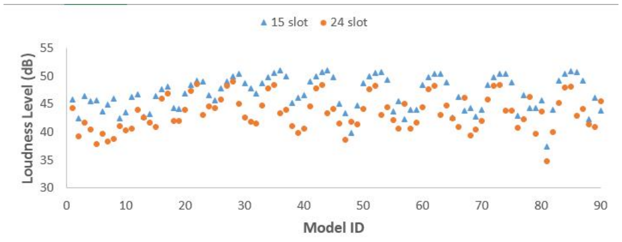

Fig. 4.8 Loudness vs. Model ID for 4 pole SynRMs at 50% Current level

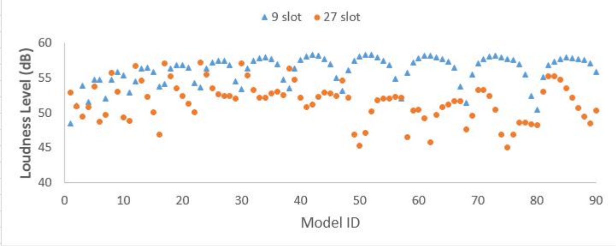

Fig. 4.9 Loudness vs. Model ID for 8 pole SynRMs at 100% Current level

frequencies from FEA are considered as the more accurate ones. The difference between the loudness results calculated with the frequencies from FEA and the ones calculated with the results from the prediction model is small. Hence we can assume that our prediction model is reasonable.

When we compared the results of the loudness from the model frequencies obtained through FEA with those obtained by the prediction model, it seems counterintuitive that the differences in the frequencies only affect the loudness a small amount. This is because the definition of the loudness value is a logarithmic function. The loudness value will not

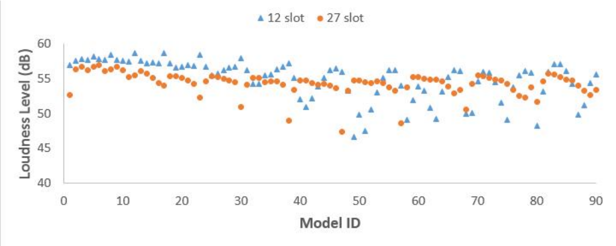

Fig. 4.10 Loudness vs. Model ID for 10 pole SynRMs at 200% Current level

be influenced enormously unless the order of magnitude of the sound pressure changes significantly. So that, a 15% error in the magnitude at a particular frequency will not have a significant effect on the result.

Moreover, we also discussed the influence on the loudness of the current level and slot number. The results show that for a SynRM, a higher current level will lead to a high loudness. And, when rotor configurations are fixed, the loudness generally increases with the lower slot numbers.

Chapter 5

Conclusion

5.1 Thesis Summary

In this thesis, we have proposed a neural network based prediction model for estimating the noise loudness level (dB) in a SynRM due to electromagnetic forces.

The noise is generated due to the electromagnetic force in the air gap between the rotor and the stator. The force impacts the stator and makes the surface of the stator have a radial displacement which leads to the vibration of the air. The air vibration generates the noise which can be heard by a human ear.

A GRNN prediction model has been developed in order to estimate the natural mode frequencies of the stator. We obtained 9/12/15/18/21/24/27/30/33 slots' stator mode frequencies from the FEA-based software, Nastran. The values computed we assume, are close to the true values. We trained the GRNN model using all the data except for the 33 slots' with a smoothing factor. Using cross validation we confirm that 0.3 is an optimal value for the smoothing factor. We also used this GRNN model to predict the 33 slots' stator natural mode frequencies and calculated the relative error rate when compared with the ones computed by FEA.

An analytical method to calculate the loudness level was introduced. First, we obtained the flux density in the air gap, then we determined the pressure wave values and the related harmonic amplitude values, then multiplied the surface area to acquire the force harmonics. With the force harmonics, the harmonics frequencies and the stator natural mode frequencies we could determine the stator's radial displacements. With the displacements, we could compute the SPL in space. Finally, from the SPL we acquired the loudness level results.

90 example SynRM models which shared the same stator configuration (33 slots) were applied in this thesis as the instances for the loudness calculation procedure. We varied the geometry parameters (carrier width & barrier width) of the rotor part to acquire different flux densities in the air gap. Using our prediction model, these example motors' stator natural mode frequencies could be estimated, while we also acquired the values through FEA. We followed the analytical method to calculate these 90 model's loudness level respectively with two sets of natural mode frequencies which are the prediction values and the FEA values. In addition, we also calculated other SynRM models with various rotor and stator configurations to discuss the relationship between loudness and other parameters, i.e the current level, and the number of slots.

5.2 Thesis Conclusion

5.2.1 GRNN Prediction Model

In the cross-validation part, which we used to confirm the optimal smoothing factor, we can see that if the target inputs (slot number, tooth width, slot depth, tooth tip thickness) are in the range of the training sets, the prediction results of the natural mode frequencies are very close to the ones from FEA. For the inputs which are beyond the training sets, such as slot number 33 (the training set slot number 9/12/15/18/21/24/27/30), the experiment results still show that the prediction is reliable. Hence the GRNN model can be assumed feasible in estimating the natural mode frequencies of the stator.

Finally an experiment was conducted to test the accuracy of the prediction model trained by different datasets.The results show that the accuracy of the GRNN model will be increased if more training sets are given.

5.2.2 Loudness Disscussion

We compared the loudness results which are calculated with the predicted mode frequencies and the ones which are calculated with the FEA mode frequencies. The two sets of results are rather close. For most of the example models, the errors are around 3 dB, which can be hardly distinguished by a human ear in the real situation. This shows that the natural mode frequencies from GRNN prediction model are reliable.

Moreover, in section 4.5 we discussed the current level and the slot number's influence on loudness. From the results and the figures we can see that as the current level increases, the loudness will increase. Additionally, loudness generally increases with the lower slot numbers.

5.3 Future Improvement

There are several works which can be done in the future.

First, due to a lack of capability we haven't applied the results to actual measurements to test the accuracy of the analytical calculation method of the loudness level. In the future, it would be useful to perform the experiments to confirm the accuracy of the approach.

Second, we can expand the training set of the GRNN prediction model. For this thesis, we used 9/12/15/18/21/24/27/30/33 slots data as the training set, while the geometric parameters (tooth width& slot depth& tang angle & tooth tip thickness) for each number of stator slots were also limited in a specific range. As we explained in Chapter 3, the more training sets that are used, more accurate the GRNN model will be. In this case, we could also develop more data from FEA to train the GRNN model.

Third, in this thesis we only developed the prediction model for estimating the natural mode frequencies of the stator. The way to obtain the air gap flux density is still through FEA-based software MagNet. If we could confirm some parameters which would predict the magnitude of the flux density, we will be able to train another prediction model in order to estimate the flux density values. Hence the computation time can be saved.

References

[1] J. F. Gieras, C. Wang, and J. C. Lai, *Noise of polyphase electric motors.* CRC press, 2005.

[2] R. Islam and I. Husain, "Analytical model for predicting noise and vibration in permanent-magnet synchronous motors," *IEEE Transactions on industry applications*, vol. 46, no. 6, pp. 2346–2354, 2010.

[3] American National Standards Institute, "American national psychoacoustical terminology," *American Standards Association*, S3.20, 1973.

[4] W. Cory, "Relationship between sound pressure and sound power levels," *Eurovent. WG*, vol. 1, 2010.

[5] M. S. Islam, R. Islam, and T. Sebastian, "Noise and vibration characteristics of permanent-magnet synchronous motors using electromagnetic and structural analyses," *IEEE Transactions on Industry Applications*, vol. 50, no. 5, pp. 3214–3222, 2014.

[6] J. F. Gieras, C. Wang, J. Lai, and N. Ertugrul, "Analytical prediction of noise of magnetic origin produced by permanent magnet brushless motors," *Electric Machines Drives Conference*, pp. 148–152, 2007.

[7] P. C. Krause, O. Wasynczuk, and S. D. Pekarek, "Electromechanical motion devices," *John Wiley & Sons*, vol. 90, 2012.

[8] J.R.Hendershot, "Electric Machine Design," http://cusp.umn.edu/machine_design.php, 2012, [Online].

[9] T. Fukami, M. Momiyama, K. Shima, R. Hanaoka, and S. Takata, "Steady-state analysis of a dual-winding reluctance generator with a multiple-barrier rotor," *IEEE Transactions on Energy Conversion*, vol. 23, no. 2, pp. 492–498, 2008.

[10] J. Kostko, "Polyphase reaction synchronous motors," *Journal of the American Institute of Electrical Engineers*, vol. 42, no. 11, pp. 1162–1168, 1923.

[11] R. R. Moghaddam, “Synchronous reluctance machine (synrm) design,” *Master, Department of Electrical Engineering Electrical Machines and Power electronics, Royal Institute of Technology, Stockholm*, 2007.

[12] D. Staton, T. Miller, and S. Wood, “Maximising the saliency ratio of the synchronous reluctance motor,” *IEE Proceedings B-Electric Power Applications*, vol. 140, no. 4, pp. 249–259, 1993.

[13] F.Gabriel, *Position Self-Sensing of Permanent-Magnet Machines using High-Frequency Signal Injection.* Brussels: VUBPRESS Brussels University Press, 2013.

[14] “Msc nastran structural analysis software,” http://www.mscsofteware.com, 2016.

[15] D. J. MacKay, *Information theory, inference and learning algorithms.* Cambridge university press, 2003.

[16] A. Castelletti, D. de Rigo, A. E. Rizzoli, R. Soncini-Sessa, and E. Weber, “A selective improvement technique for fastening neuro-dynamic programming in water resource network management,” *IFAC Proceedings Volumes*, vol. 38, no. 1, pp. 7–12, 2005.

[17] C. Ferreira, “Gene expression programming: mathematical modeling by an artificial intelligence,” *Springer*, vol. 21, 2006.

[18] Y. Da and G. Xiurun, “An improved pso-based ann with simulated annealing technique,” *Neurocomputing*, vol. 63, pp. 527–533, 2005.

[19] J. Wu and E. Chen, “A novel nonparametric regression ensemble for rainfall forecasting using particle swarm optimization technique coupled with artificial neural network,” *International Symposium on Neural Networks*, pp. 49–58, 2009.

[20] D. F. Specht, “A general regression neural network,” *IEEE Transactions on Neural Networks*, vol. 2, no. 6, pp. 568–576, 1991.

[21] R. L. Kendrick, D. S. Acton, and A. Duncan, “Phase-diversity wave-front sensor for imaging systems,” *Applied Optics*, vol. 33, no. 27, pp. 6533–6546, 1994.

[22] T. P. Williams and N. Gucunski, “Neural networks for backcalculation of moduli from sasw test,” *Journal of Computing in Civil Engineering*, vol. 9, no. 1, pp. 1–8, 1995.

[23] B. D. Baker, “Can flexible non-linear modeling tell us anything new about educational productivity?” *Economics of Education Review*, vol. 20, no. 1, pp. 81–92, 2001.

[24] S. Ibrić, M. Jovanović, Z. Djurić, J. Parojčić, and L. Solomun, “The application of generalized regression neural network in the modeling and optimization of aspirin extended release tablets with eudragit® rs po as matrix substance,” *Journal of Controlled Release*, vol. 82, no. 2, pp. 213–222, 2002.

[25] D. a. N. W. N.S.Visen, J.Paliwal, "Specialist neural networks for cereal grain classification," *Biosystems Engineering*, vol. 82, no. 2, pp. 151–159, 2002.

[26] S. Jeyamkondan, D. Jayas, and R. Holley, "Microbial growth modelling with artificial neural networks," *International Journal of Food Microbiology*, vol. 64, no. 3, pp. 343–354, 2001.

[27] J. Li, J.-h. Cheng, J.-y. Shi, and F. Huang, "Brief introduction of back propagation (bp) neural network algorithm and its improvement," in *Advances in Computer Science and Information Engineering.* Springer, 2012, pp. 553–558.

[28] H. Schløler and U. Hartmann, "Mapping neural network derived from the parzen window estimator," *Neural Networks*, vol. 5, no. 6, pp. 903–909, 1992.

[29] M. Anwar and O. Husain, "Radial force calculation and acoustic noise prediction in switched reluctance machines," *IEEE Transactions on Industry Applications*, vol. 36, no. 6, pp. 1589–1597, 2000.

[30] D. Cameron, J. Lang, and S. Umans, "The origin of acoustic noise in variable-reluctance motors," *Industry Applications Society Annual Meeting, 1989., Conference Record of the 1989 IEEE*, pp. 108–115, 1989.

[31] M. H. Mohammadi, *Rotor Design Optimization of Permanent Magnet-Assisted Synchronous Reluctance Machines for Traction Applications.* McGill University Master Dissertation, 2015.

[32] "Magnet 3d electromagnetic analysis software," http://www.infolytica.ca, 2016.

[33] R. Girgis and S. Vermas, "Method for accurate determination of resonant frequencies and vibration behaviour of stators of electrical machines," *IEE Proceedings B-Electric Power Applications*, vol. 128, no. 1, p. 1, 1981.

[34] S. Yang, "Low-noise electrical motors," *Oxford University Press, USA*, vol. 13, 1981.